

# Wave Impact Loads by MPS Method with an Improved Pressure Source Term

by Liang-Yee Cheng\*  
Cezar Augusto Bellezi\*

Rubens Augusto Amaro Junior\*

**Key Words:** Pressure Oscillation, Hydrodynamic Loads, Source Term, Particle-based Method, MPS

## 1. INTRODUCTION

Wave induced motions and loads associated to violent free surface flows and fluid-structure interaction (FSI) phenomena are highly non-linear hydrodynamic problems of great concern to coastal or offshore structures due to safety and operational issues.

In recent years, Lagrangian particle-based methods have opened new perspective for the investigation of strong FSI problems with large free surface deformation<sup>1,2)</sup>. Nevertheless, spurious oscillation of computed pressure is one of the main issues of the particle-based methods. The approaches to achieve more stable computation are: enhancement of regular particle distributions, which has computational cost of resetting the particle positions<sup>3)</sup>; modified and/or high-order differential operators<sup>4,5)</sup>; and new formulations for the source term of pressure Poisson equation (PPE), by combining incompressibility conditions<sup>6,7)</sup> or introducing higher order source terms<sup>8)</sup>.

Despite promising in mitigation the oscillations, in the results obtained by most of the existing solutions the spurious oscillations tend to increase with the decrease of time step, with the stability range sensitive to time domain discretization. The present work adopts new source terms for the PPE based on a correction factor between numerical and physical time scale, which is derived from the momentum conservation regarding collisions in particle-level. For the purpose of the investigation, the Moving Particle Semi-implicit (MPS) method<sup>1)</sup> is considered. In addition, a high-order stabilized gradient model<sup>9)</sup> is adopted to mitigate the effect of nonuniform particle distribution, thus reducing the numerical wave attenuation inherent of the original MPS model. In order to evaluate the performance of the proposed approach when applied to violent free surface flows and FSI phenomena, numerical results are compared to available experimental measurements, particularly regarding two cases: nonlinear wave impacts on the vertical wall<sup>10)</sup> and floating body under the action of wave maker<sup>11)</sup>.

## 2. NUMERICAL METHOD

### 2.1 Moving Particle Semi-implicit

The Moving Particle Semi-implicit (MPS) method solves the governing equations of continuum by replacing the differential operators by discrete differential operators derived

based on a weight function ( $\omega_{ij}$ ). To solve the incompressible viscous flow, a semi-implicit algorithm is used in the MPS method. At first, predictions of the particles velocity and position are carried out explicitly by using viscosity and external forces terms of the momentum conservation. Then the pressure of all particles is obtained implicitly by solving a linear system of PPE considering the particle number density (PND) criterion<sup>1)</sup> as follows:

$$\langle \nabla^2 P \rangle_i^{t+\Delta t} - \frac{\alpha \rho}{\Delta t^2} P_i^{t+\Delta t} = \gamma \frac{\rho}{\Delta t^2} \left( \frac{n_0 - n_i^*}{n_0} \right), \quad (1)$$

where  $n_0$  stands the initial PND,  $n_i^*$  is the PND of the particle distribution after the explicit calculations,  $\rho$  denotes the fluid density,  $\Delta t$  is the time step,  $\alpha$  represents a compressibility factor and  $\gamma$  is a relaxation coefficient to reduce spurious pressure oscillations. The PND of a particle  $i$  is proportional to the fluid density and is obtained as the summation of the weight of all neighbor particles. After solving the PPE, the fluid particle velocity and position are updated based on the pressure gradient<sup>1)</sup>

$$\langle \nabla P \rangle_i = \frac{d}{n^0} \sum_{j \neq i} \frac{P_j - \hat{P}_i}{\|\mathbf{r}_{ij}\|^2} \mathbf{r}_{ij} \omega_{ij}, \quad (2)$$

where  $d$  is the number of spatial dimensions and  $\hat{P}_i$  is the minimum pressure between the neighborhood of the particle  $i$ , and vector distance  $\mathbf{r}_{ij} = \mathbf{r}_j - \mathbf{r}_i$ .

To prevent instability issue induced by attractive pressure and reduces the effect of nonuniform particle distribution, Wang et al.<sup>9)</sup> introduced a corrective matrix in Eq. (2) and obtained the following stabilized pressure gradient model

$$\langle \nabla P \rangle_i = \mathbf{C}_i \sum_{j \neq i} \frac{P_j - \hat{P}_i}{\|\mathbf{r}_{ij}\|^2} \mathbf{r}_{ij} \omega_{ij}, \quad (3)$$

where  $\mathbf{C}_i$  is the corrective matrix:

$$\mathbf{C}_i = \left[ \sum_{j \neq i} \omega_{ij} \frac{\mathbf{r}_{ij}}{\|\mathbf{r}_{ij}\|} \otimes \frac{\mathbf{r}_{ij}^T}{\|\mathbf{r}_{ij}\|} \right]^{-1}. \quad (4)$$

Then the velocity of the particles is updated by using the pressure gradient term of the momentum conservation and the new positions of the particles are obtained.

The method adopts Dirichlet boundary conditions for pressure and motion. The motion boundary conditions are imposed to the solids, modeled as particles as well, during the explicit step of the method. The Dirichlet pressure boundary condition is imposed to the particles identified as free surface and it is considered during the implicit step of the method. In the present work the NPCD method<sup>12)</sup> is adopted to identify the free surface particles.

### 2.2 Correction factor for PPE

Numerically, the duration of time discontinuous phenomena such as collisions or impacts is about the simulation time step

\* University of São Paulo, Brazil

Received (Filed by JASNAOE)

Published (Filed by JASNAOE)

Read at the spring/autumn meeting (Reformed by JASNAOE)

©The Japan Society of Naval Architects and Ocean Engineers  
Japan

$\Delta t$  because the change of the status prior and after the event is only detected and processed in the instant when the change occurs. Nevertheless, considering successive collisions or impacts in a continuum with minimal spatial resolution  $l_0$ , the intervals between the successive collisions are about the physical time interval  $\delta t = l_0/c_s$ , where  $c_s$  is propagation velocity. In explicit numerical scheme, due to the CFL stability condition, it is clear that  $\Delta t < \delta t$ . This means that the successive collisions or impacts that physically must last  $\delta t$  are numerically shortened to  $\Delta t$ .

As the momentum conservation is assured by the governing equations, the impulse  $I$  of a collision or impact computed numerically or recorded physically should be the same. So, the integration of the computed loads ( $F_n$ ) in the interval  $[t, t + \Delta t]$  must be equivalent to the integration of the physical collision loads ( $F_p$ ) in  $[t, t + \delta t]$ . As result, the ratio between the numerical and the physical collision loads ( $F_n/F_p$ ) yields the relation  $\Delta t = C_r \delta t$ . Therefore, the imposition of the stability criterion leads to much higher numerical pulses than the physical ones, with the amplification coefficient of  $1/C_r$ . In the other words, as the duration of the numerical pulses is much shorter than the physical ones, each of these discrete impacts shows a much larger magnitude of the impulsive loads.

Moreover, as a result of the mismatch, the solution is inconsistent in time domain, with peak values very sensitive to  $\Delta t$ , because the magnitude of the numerical collision loads  $F_n \rightarrow \infty$  when the numerical time step  $\Delta t \rightarrow 0$ . This issue on the numerical modeling in the computation of time discontinuous phenomena was observed by Cheng et al.<sup>13</sup>, who proposed the application of the Courant number as a correction factor for stable assessment of impulsive loads in mesh-based methods.

In the present work, considering the motions and collisions in particle-level, the solution proposed to mitigate spurious pressure oscillation that occur in particle-based simulations even for non-impulsive loads is the introduction of Courant number  $C_r = (c_s \Delta t)/l_0$  as a correction factor in the pressure computation. Instead of using the numerical time step  $\Delta t$  in the source term (Eq. (1)), the physical time step  $\delta t = l_0/c_s$  is preferred to adjust both the magnitude and duration of the impulses. This is the same as imposing  $\gamma = C_r^2 = (c_s \Delta t/l_0)^2$  in Eq. (1), so that:

$$\langle \nabla^2 P \rangle_i^{t+\Delta t} - \frac{\alpha \rho}{\Delta t^2} P_i^{t+\Delta t} = c_s^2 \frac{\rho}{l_0^2} \left( \frac{n_0 - n_i^*}{n_0} \right). \quad (5)$$

Another incompressible condition considered in the source term is that the divergence of the velocity field should be zero, as proposed by Tanaka e Matsunaga<sup>7</sup>:

$$\langle \nabla^2 P \rangle_i^{t+\Delta t} - \frac{\alpha \rho}{\Delta t^2} P_i^{t+\Delta t} = \gamma \frac{\rho}{\Delta t^2} \left( \frac{n_0 - n_i^t}{n_0} \right) + \frac{\rho}{\Delta t} \nabla \cdot \mathbf{u}^*. \quad (6)$$

The introduction of the relaxation coefficient  $\gamma = C_r^2$  and by using the physical time  $\delta t$ , a new source term considering the divergence of the velocity is obtained:

$$\langle \nabla^2 P \rangle_i^{t+\Delta t} - \frac{\alpha \rho}{\Delta t^2} P_i^{t+\Delta t} = c_s^2 \frac{\rho}{l_0^2} \left( \frac{n_0 - n_i^t}{n_0} \right) + c_s \frac{\rho}{l_0} \nabla \cdot \mathbf{u}^*. \quad (7)$$

The list of the original and the improved source terms investigated in the present paper is shown in Tab. 1.

Table 1 Description of the original and proposed source terms.

Source term	Abbreviation
Original PND deviation with 0 <sup>th</sup> order gradient. Eqs. (1) and (2)	O-PND
Proposed PND deviation with 0 <sup>th</sup> order gradient. Eqs. (5) and (2)	P-PND
Original PND deviation and divergence-free condition with 0 <sup>th</sup> order gradient. Eqs. (6) and (2)	O-PND-DF
Proposed PND deviation and divergence-free condition with 0 <sup>th</sup> order gradient. Eqs. (7) and (2)	P-PND-DF
Original PND deviation and divergence-free condition with high-order gradient. Eqs. (6) and (3)	O-PND-DF-HG
Proposed PND deviation and divergence-free condition with high-order gradient. Eqs. (7) and (3)	P-PND-DF-HG

### 3. RESULTS

#### 3.1 Wave impacts on the vertical wall

Pressure on the wall and wave elevation computed by original MPS and proposed approach are compared with the experimental results provided by Didier et al.<sup>10</sup>. The main dimensions of the problem are shown in Fig. 1. The wave maker motion is governed by  $x(t) = -A \sin \omega t$ , where  $A = 0.05048$  m and  $\omega = 2\pi/1.3$  rad/s. The initial distance between particles  $l_0 = 0.01$  m (15124 particles in total) is adopted. The simulation parameters used here are: effective radius  $r_e = 2.1l_0$  for the gradient and divergence operators,  $r_e = 4.0l_0$  for the Laplacian operator, relaxation coefficient  $\gamma = 0.01$ , propagation velocity  $c_s = 2$  m/s and compressibility factor  $\alpha = 10^{-8}$  kg<sup>-1</sup>ms<sup>2</sup>.

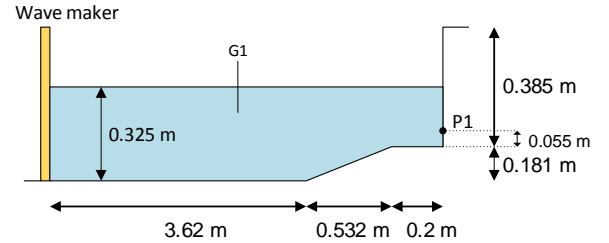


Fig. 1 Main dimensions and sensors of wave impact on wall.

Figures 2, 3 and 4 present the wave impact pressure at P1 considering the time steps of  $\Delta t = 0.002$  and  $0.0002$  s. According to Figs. 2, 3 and 4, the adoption of divergence-free condition contributes to reduce the pressure oscillation. As indicated in Fig. 4, the use of the high-order gradient reproduces the pressure amplitude after the first cycle in very good agreement with the experimental result by Didier et al.<sup>10</sup>, while the use of 0<sup>th</sup> order gradient underestimates the pressure amplitude, indicating that high-order gradient diminish the numerical dissipation and is highly recommended for long time simulations. However, the decrease of time step  $\Delta t$  increases the amplitude of pressure oscillations computed by using original source terms O-PND, O-PND-DF and O-PND-DF-HG, as mentioned in Section 2.2. On the other hand, spurious oscillation is mitigated by using the proposed approach, even when the high-order gradient is adopted. With the straightforward calibration provided by using the propagation speed of the perturbations  $c_s$ , the improvement is remarkably effective for small time steps and more stable pressures were computed in a wide range of time steps.

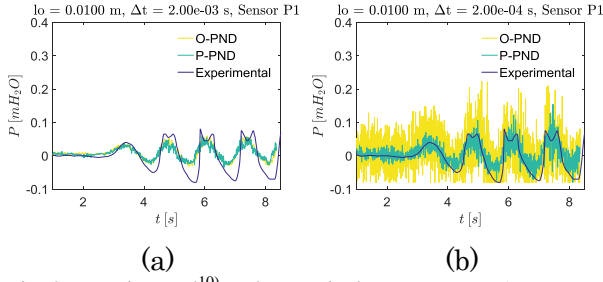


Fig. 2 Experimental<sup>10)</sup> and numerical pressures at P1 computed with O-PND and P-PND. Simulations with  $l_0 = 0.01$  m, (a)  $\Delta t = 2 \times 10^{-3}$  s and (b)  $\Delta t = 2 \times 10^{-4}$  s.

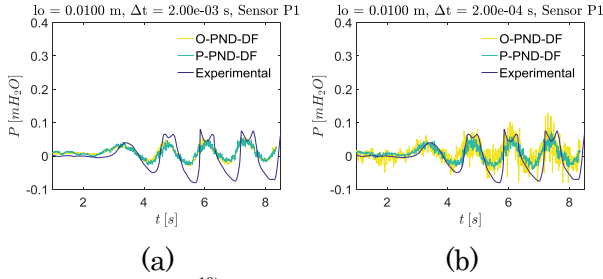


Fig. 3 Experimental<sup>10)</sup> and numerical pressures at P1 computed with O-PND-DF and P-PND-DF. Simulations with  $l_0 = 0.01$  m, (a)  $\Delta t = 2 \times 10^{-3}$  s and (b)  $\Delta t = 2 \times 10^{-4}$  s.

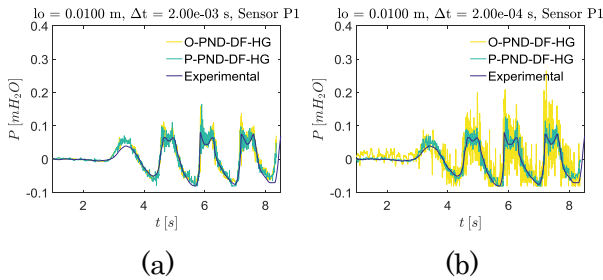


Fig. 4 Experimental<sup>10)</sup> and numerical pressures at P1 computed with O-PND-DF-HG and P-PND-DF-HG. Simulations with  $l_0 = 0.01$  m, (a)  $\Delta t = 2 \times 10^{-3}$  s and (b)  $\Delta t = 2 \times 10^{-4}$  s.

Images of the pressure distribution in wave impact simulation computed by O-PND and P-PND-DF-HG are compared in Fig. 5. The color scale is associated to pressure field. The simulation computed by O-PND leads to an irregular pressure field with numerical oscillations and wave energy dissipation. On the other hand, smoother pressure field were obtained by using P-PND-DF-HG.

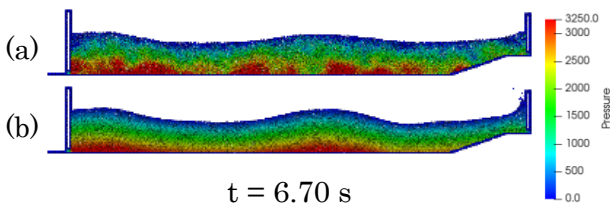


Fig. 5 Pressure fields computed by using source (a) O-PND and (b) P-PND-DF-HG at  $t = 6.70$  s.

Figure 6 shows the wave elevation at wave gauge G1, 2.643 m from the initial position of the wave maker. The wave elevations computed by using the original MPS (O-PND) and proposed source terms P-PND and P-PND-DF are attenuated after one or two wavelengths, whereas the proposed source term with high-order gradient (P-PND-DF-HG) decreases the numerical wave dissipation, therefore reproducing the wave

elevation in better agreement with the experimental one.

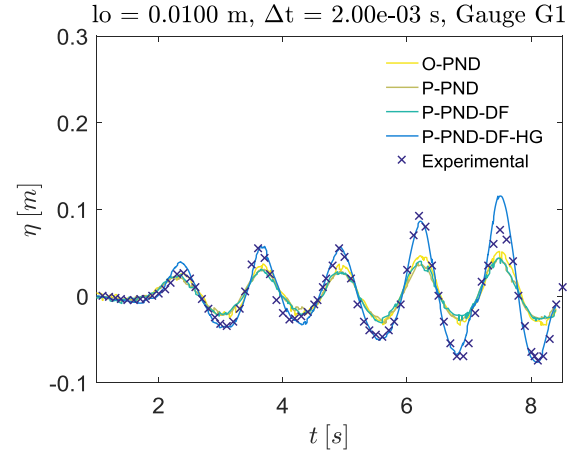


Fig. 6 Experimental<sup>10)</sup> and numerical wave elevations at G1.

### 3.2 Floating body under the action of wave maker

Wave elevation and floating body motions computed by original (O-PND) and proposed (P-PND-DF-HG) source terms are compared with the experimental results available in Hadžića et al<sup>11)</sup>. The floating body is a rectangular prism 0.1 m long, 0.05 m high and 0.29 m wide, with density of  $680 \text{ kg/m}^3$ . The mass of the body is 0.986 kg in 3D, but the simulation is performed in 2D and the mass of the body adopted is 3.4 kg. Considering the floating body as a homogeneous solid, the moment of inertia  $I = 3.54 \times 10^{-3} \text{ kg m}^2$  is considered. The main dimensions of the experiment are shown in Fig. 7. The time history of the wave maker angle motion<sup>11)</sup> is plotted in Fig. 8. The initial distance between particles  $l_0 = 0.005$  m (98390 particles in total) is adopted. The simulation parameters used here are: effective radius  $r_e = 2.1l_0$  for the gradient and divergence operators,  $r_e = 4.0l_0$  for the Laplacian operator, relaxation coefficient  $\gamma = 0.01$ , propagation velocity  $c_s = 2 \text{ m/s}$  and compressibility factor  $\alpha = 10^{-8} \text{ kg}^{-1} \text{ ms}^2$ .

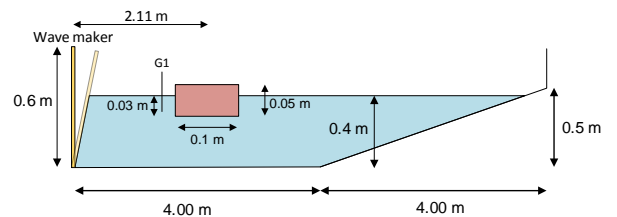


Fig. 7 Main dimensions and gauges of floating body case.

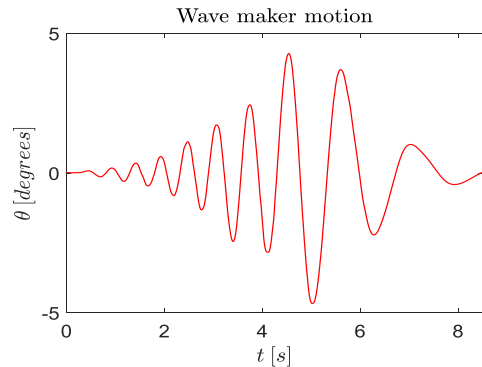


Fig. 8 Wave maker motion<sup>11)</sup>.

The experimental and numerical wave elevation at G1,

before the location of the body ( $x = 1.16\text{m}$ ) is shown in Fig. 9. As in the previous case, a very good agreement between numerical results computed by using the proposed approach (P-PND-DF-HG) and experimental data is obtained concerning the wave elevation at G1. In contrast, numerical result computed by original MPS shows large energy dissipation, thus resulting in a lower wave elevation compared to experimental one.

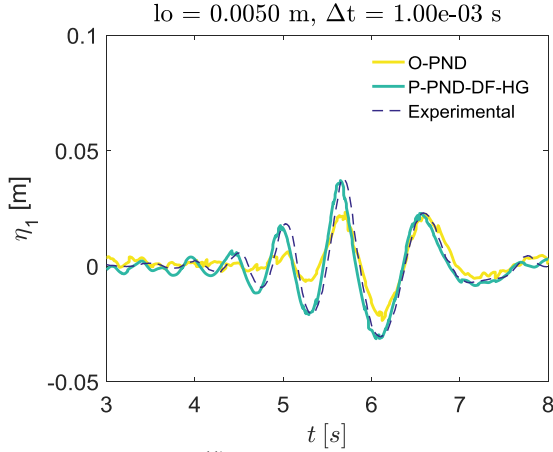


Fig. 9 Experimental<sup>11)</sup> and numerical wave elevations at G1.

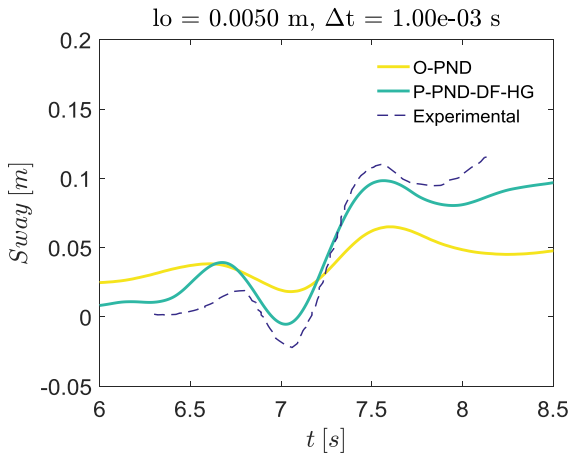


Fig. 10 Experimental<sup>11)</sup> and numerical sway motions of the floating body.

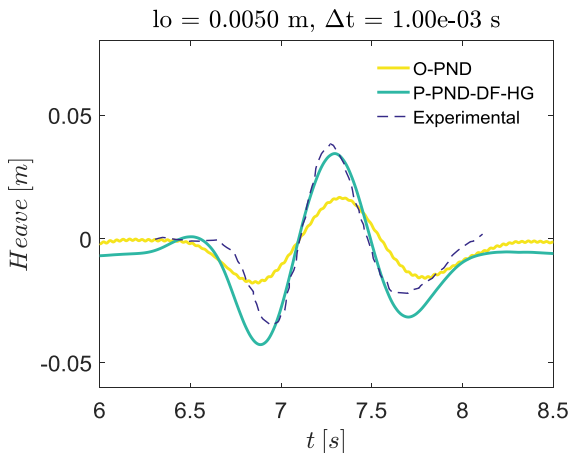
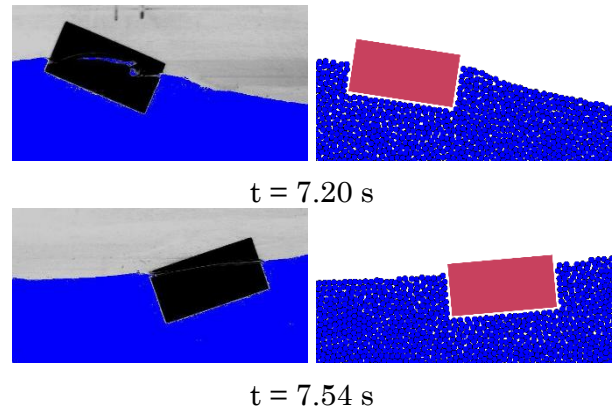


Fig. 11 Experimental<sup>11)</sup> and numerical heave motions of the floating body.

Figures 10 and 11 present, respectively, the experimental and numerical time series of the sway and heave motions of

the floating body. The numerical wave dissipation present in original MPS leads to attenuation of motions. On the other hand, the improvements achieved by P-PND-DF-HG, reducing the pressure oscillations and wave dissipation, provide computed sway and heave motions in good agreements with experimental ones.

Figure 12 presents snapshots of the experimental and numerical wave and floating body motions at the instants  $t = 7.20\text{ s}$  and  $t = 7.54\text{ s}$ . Numerical and experimental free surface motions are in very good agreements. Concerning the floating body motions, a good agreement between experimental and computed sway and heave motions are obtained. However, experimental and computational roll motions present some discrepancies. Compared to experimental results, slightly smaller rotational motions are computed at  $t = 7.20\text{ s}$  and  $t = 7.54\text{ s}$ .



Experimental P-PND-DF-HG  
Fig. 12. Experimental (left) and numerical (right) wave and floating body motion at  $t = 7.20\text{ s}$  (top) and  $t = 7.54\text{ s}$  (bottom).

#### 4. CONCLUSIONS

In the present work, new source terms for the pressure Poisson equation (PPE) are derived from the viewpoint of the momentum conservation of particle-level collisions, and their performance for mitigation of the spurious pressure oscillation were analyzed with respect to several aspects of the numerical computations. In addition, a high-order stabilized gradient model is adopted, thus reducing the numerical wave attenuation inherent of the original MPS model.

Two examples are studied to demonstrate the effectiveness of the proposed approach when applied to violent free surface flows and FSI phenomena. For the first case, consisting of a wave impact on seawall, the proposed approach drastically suppressed the unphysical pressure oscillations, with pressure oscillations almost independent to time steps. The wave elevation and impact pressure computed by the proposed approach are in very good agreement with experimental results, when proposed source term combining zero variation of the density and the divergence-free condition with high-order gradient (P-PND-DF-HG) is applied. For the second example of a floating body under the action of wave maker, the wave elevations are accurately computed by the proposed approach and the floating body motions are in good agreement with available experimental results.

In comparison to the other strategies, the proposed approach has much simpler implementation and is more computationally

efficient.

### ACKNOWLEDGMENT

This material is based upon research supported by the Office of Naval Research Global under the Award Number: N62909-16-1-2181. This study was financed in part by the Coordenação de Aperfeiçoamento de Pessoal de Nível Superior - Brasil (CAPES) - Finance Code 001, for the doctorate scholarship of Rubens Augusto Amaro Junior and Cezar Augusto Bellezi. The authors are also grateful to Petrobras for financial support on the development of the MPS/TPN-USP simulation system based on MPS method.

### REFERENCES

- 1) S. Koshizuka and Y. Oka: Moving-particle semi-implicit method for fragmentation of incompressible fluid, *Nuclear Science and Engineering*, vol. 123, pp. 421-434, 1996.
- 2) E. Y. M. Lo and S. Shao: Simulation of near-shore solitary wave mechanics by an incompressible SPH method, *Applied Ocean Research*, vol. 24, no. 5, pp. 275-286, 2002.
- 3) J. Wang and X. Zhang: Modified Particle Method with integral Navier–Stokes formulation for incompressible flows, *Journal of Computational Physics*, vol. 366, no. 1, pp. 1-13, 2018.
- 4) P. W. Randles and L. D. Libersky: Smoothed Particle Hydrodynamics: Some recent improvements and applications, *Computer Methods in Applied Mechanics and Engineering*, vol. 139, no. 1-4, pp. 375-408, 1996.
- 5) T. Tamai and S. Koshizuka: Least squares moving particle semi-implicit method, *Computational Particle Mechanics*, vol. 1, no. 3, pp. 277-305, 2014.
- 6) I. Hirokazu: Numerical analysis of fragmentation processes in vapor explosion using particle method., 1999.
- 7) M. Tanaka and T. Masunaga: Stabilization and smoothing of pressure in MPS method by Quasi-Compressibility, *Journal of Computational Physics*, vol. 229, no. 11, pp. 4279-4290, 2010.
- 8) A. Khayyer and H. Gotoh: Modified Moving Particle Semi-implicit methods for the prediction of 2D wave impact pressure, *Coastal Engineering*, vol. 56, no. 4, pp. 419-440, 2009.
- 9) L. Wang et al.: Improvement of moving particle semi-implicit method for simulation of progressive water waves, *International Journal for Numerical Methods in Fluids*, vol. 85, no. 2, pp. 69-89, 2017.
- 10) E. Didier et al.: Wave interaction with a vertical wall: SPH numerical and experimental modeling, *Ocean Engineering*, vol. 88, pp. 330–341, 2014.
- 11) I. Hadžića et al: Computation of flow-induced motion of floating bodies, *Applied Mathematical Modelling*, vol. 29, no. 12, pp. 1196-1210, 2005.
- 12) M. M. Tsukamoto et al.: Fluid interface detection technique based on neighborhood particles centroid deviation (NPCD) for particle methods, *International Journal for Numerical Methods in Fluids*, vol. 82, pp. 148-168, 2016.
- 13) L.-Y. Cheng and M. Arai: A Numerical treatment of the boundary conditions for stable assessment of hydrodynamic impact pressure, *OMAE2002*, 2002.